Draft version February 5, 2008
Preprint typeset using LaTeX style emulateapj v. 6/22/04

POWER SPECTRUM OF COSMIC MOMENTUM FIELD MEASURED FROM THE SFI GALAXY SAMPLE

Chan-Gyung Park and Changbom Park
Korea Institute for Advanced Study, 130-722, Seoul, Korea
(Received July 12, 2005; Accepted September 18, 2005)
Draft version February 5, 2008

ABSTRACT

We have measured the cosmic momentum power spectrum from the peculiar velocities of galaxies in the SFI sample. The SFI catalog contains field spiral galaxies with radial peculiar velocities derived from the I-band Tully-Fisher relation. As a natural measure of the large-scale peculiar velocity field, we use the cosmic momentum field that is defined as the peculiar velocity field weighted by local number of galaxies. We have shown that the momentum power spectrum can be derived from the density power spectrum for the constant linear biasing of galaxy formation, which makes it possible to estimate $\beta_{\rm S} = \Omega_m^{0.6}/b_{\rm S}$ parameter precisely where Ω_m is the matter density parameter and $b_{\rm S}$ is the bias factor for optical spiral galaxies. At each wavenumber k we estimate $\beta_{\rm S}(k)$ as the ratio of the measured to the derived momentum power over a wide range of scales ($0.026\ h^{-1}{\rm Mpc} \lesssim k \lesssim 0.157\ h^{-1}{\rm Mpc}$) that spans the linear to the quasi-linear regimes. The estimated $\beta_{\rm S}(k)$'s have stable values around 0.5, which demonstrates the constancy of $\beta_{\rm S}$ parameter at scales down to $40\ h^{-1}$Mpc. We have obtained $\beta_{\rm S} = 0.49^{+0.08}_{-0.05}$ or $\Omega_m = 0.30^{+0.09}_{-0.05} b_{\rm S}^{5/3}$, and the amplitude of mass fluctuation as $\sigma_8 \Omega_m^{0.6} = 0.56^{+0.27}_{-0.21}$. The 68% confidence limits include the cosmic variance. We have also estimated the mass density power spectrum. For example, at $k = 0.1047\ h{\rm Mpc}^{-1}$ ($\lambda = 60\ h^{-1}$Mpc) we measure $\Omega_m^{1.2} P_\delta(k) = (2.51^{+0.91}_{-0.94}) \times 10^3\ (h^{-1}{\rm Mpc})^3$, which is lower compared to the high-amplitude power spectra found from the previous maximum likelihood analyses of peculiar velocity samples like Mark III, SFI, and ENEAR.

Subject headings: cosmology: theory — cosmology: large-scale structure of universe

1. INTRODUCTION

Peculiar motions of galaxies in the nearby Universe are very powerful tool for examining the underlying mass fluctuations on large scales. The galaxy peculiar velocity directly probes the large-scale matter density field, and thus gives biasing information of galaxy distribution. The advantage in using the peculiar velocity data is that we can explore the large-scale structures in the real space rather than in the redshift space, without redshift space distortion. On the other hand, the galaxy peculiar velocities or the absolute distances have large errors proportional to distance because the absolute distance is usually inaccurately measured compared with the redshift. For this reason peculiar velocity samples are in general much smaller than redshift survey samples. In spite of this disadvantage, the peculiar velocity sample is very useful since the observed velocity field contains information on larger scales compared with the density field in a given survey volume.

In the study of peculiar velocity field, homogeneous peculiar velocity sample with well-defined selection criteria is essential because the sparse and inhomogeneous sample significantly induces biases in estimating physical parameters. Over a decade or so there has been major progress in the peculiar velocity studies. Observationally, there has been a dramatic improvement with the completion of large Tully-Fisher (TF) and $D_{\rm n}$–σ redshift-distance surveys in both hemispheres. Those are the Mark III catalog (Willick et al. 1997a) that contains about 3,300 spiral and elliptical galaxies, the SFI catalog (Giovanelli et al. 1994) with about 1300 late-type spiral galaxies with I-band TF distance estimates, and the ENEAR catalog (da Costa et al. 2000b) containing about 1400 early-type galaxies with $D_{\rm n}$–σ distances. Recently, new distance indicators such as the Type Ia supernovae (Riess et al. 1997; Radburn-Smith et al. 2004) and the surface brightness fluctuation of the early-type galaxies (Blakeslee et al. 1999) have been used in the peculiar velocity study.

Theoretically, there have been many works on the peculiar velocity fields (Strauss & Willick 1995; Zaroubi 2002 for a review). The galaxy peculiar velocities have been used to reconstruct the three-dimensional velocity field or the real-space matter density field of the local Universe (e.g., da Costa et al. 1996; Dekel et al. 1999), and to estimate the amplitude of mass fluctuation and/or $\beta = \Omega_m^{0.6}/b$ parameter, where b is the linear bias factor. Among the many analysis methods that have been developed and applied to the observational data, one of the major development has been the POTENT method (Bertschinger et al. 1990; Dekel et al. 1999) which reconstructs the smoothed three-dimensional peculiar velocity field from the observed radial velocity data. As a new method of estimating β parameter accurately, Park (2000, hereafter P00) has introduced the cosmic momentum field and developed the momentum power spectrum analysis method which does not require a smoothing of galaxy peculiar velocities. Other studies have applied the velocity correlation function statistic (Górski et al. 1989; Borgani et al. 2000a,b), the maximum likelihood (ML) method (Freudling et al. 1999; Silberman et al. 2001), the orthogonal mode expansion (OME) method (Nusser & Davis 1995; da Costa et al. 1998), Wiener filtering method (Zaroubi, Hoffman, & Dekel 1999),

Electronic address: parkc@kias.re.kr;cbp@kias.re.kr

the unbiased minimal variance (UMV) estimator (Zaroubi et al. 2002), the optimal moment expansion method (Watkins et al. 2002), and the pairwise velocity method (Feldman et al. 2003). Considerable efforts have been made to estimate the β parameter from the comparison of mass density field derived from the observed radial velocities with the observed galaxy density field from the redshift survey (δ-δ comparison; Sigad et al. 1998), or from the direct comparison of the observed peculiar velocity field with that derived from the galaxy redshift survey (v-v comparison; e.g., see Zaroubi et al. 2002, references therein).

In this paper, we estimate the β parameter and the amplitude of mass fluctuation from the peculiar velocities of the SFI galaxy sample by measuring the momentum and density power spectra. The outline of this paper is as follows. In §2, we briefly review the cosmic momentum field. Description and data reduction of the SFI galaxy sample are given in §3. In §4, we measure the density and momentum power spectra from the SFI data. Measurements of β parameter and the amplitude of mass fluctuation are given in §5. We discuss our results in §6. Throughout this paper, in calculating the real-space distance from the redshift or the recession velocity, we assume a flat ΛCDM universe with matter and dark energy density parameters $\Omega_m = 0.27$ and $\Omega_\Lambda = 0.73$, respectively. For the present value of the Hubble parameter, we use $H_0 = 100h$ km/s/Mpc.

2. COSMIC MOMENTUM FIELD

This section summarizes the cosmic momentum field. For complete description we refer to P00. The cosmic momentum field is defined as the peculiar velocity field $\boldsymbol{v}$ weighted by local density $\rho/\bar{\rho}$:

$$\boldsymbol{p} \equiv \frac{\rho}{\bar{\rho}}\boldsymbol{v} = (1+\delta)\boldsymbol{v}. \tag{1}$$

Here $\delta = (\rho - \bar{\rho})/\bar{\rho}$ is the dimensionless density contrast. The cosmic momentum $\boldsymbol{p}$ defined here has the dimension of velocity and is equal to $\boldsymbol{v}$ in the linear regime ($|\delta| \ll 1$).

To compare the observed peculiar velocities of galaxies with cosmological models we measure correlation function (CF) or power spectrum (PS) of the momentum field. Suppose the matter over-density $\delta(\boldsymbol{x})$ and the peculiar velocity $\boldsymbol{v}(\boldsymbol{x})$ fields are homogeneous and isotropic random fields. Given a momentum correlation tensor $\xi^p_{ij}(r) = \langle p_i(\boldsymbol{x}) p_j(\boldsymbol{x}+\boldsymbol{r})\rangle$, we define a power spectral tensor $P^p_{ij}(k)$ as

$$P^p_{ij}(k) \equiv \int d^3r \xi^p_{ij}(r) e^{i\boldsymbol{k}\cdot\boldsymbol{r}}. \tag{2}$$

With this definition, $P^p_{ij}(k)$ has an unit of [velocity]^2 × [volume], conventionally km^{2}s^{-2}(h^{-1}Mpc)^3. We call its trace $P_p(k) \equiv P^p_{ii}(k) = \int d^3x \xi_p(r) e^{i\boldsymbol{k}\cdot\boldsymbol{x}}$ as the PS of the momentum field, where $\xi_p(r) \equiv \xi^p_{ii}(r) = \langle \boldsymbol{p}(\boldsymbol{x})\cdot\boldsymbol{p}(\boldsymbol{x}+\boldsymbol{r})\rangle$ is the dot-product CF of the momentum field.

What we directly measure in a galaxy peculiar velocity survey is the radial component of peculiar velocities at the locations of galaxies. The radial component of momentum, the physical observable in our analysis, is the galaxy number-weighted quantity $p_r(\boldsymbol{x}) = u(\boldsymbol{x})n(\boldsymbol{x})/\bar{n}$, where the radial peculiar velocity $u(\boldsymbol{x})$ is caused by the total matter field and $n(\boldsymbol{x})/\bar{n}$ represents the distribution of galaxies. With the isotropy of the momentum field and the far-field approximation, P00 obtained

$$P_p(k) \approx 3P_{p_r}(k). \tag{3}$$

The three-dimensional momentum PS can be measured from the PS of radial component of momentum $P_{p_r}(k)$. This property can be directly applied to the all-sky peculiar velocity survey data. By comparing the PS of the total momentum with those of the radial component of the momentum vector observed at a corner or at the center of the simulation cube, P00 has demonstrated that equation (3) is actually very accurate over wide scales when the cosmic variance and observational uncertainties in the PS are taken into account. However, at scales corresponding to the fundamental modes within the survey volume, equation (3) holds only approximately.

If the velocity field is irrotational (curl-free), Fourier mode of velocity field in the linear regime becomes

$$\boldsymbol{v}(\boldsymbol{k}) = -i(DHf)\frac{\boldsymbol{k}}{k^2}\tilde{\delta}(\boldsymbol{k}), \tag{4}$$

where $D(t)$ is the linear growth factor as in $\delta(\boldsymbol{k};t) = D(t)\tilde{\delta}(\boldsymbol{k})$, $H \equiv \dot{a}/a$ is the Hubble parameter, $a(t)$ is the expansion factor, and $f(\Omega_m, \Omega_\Lambda) \equiv d\ln D/d\ln a \simeq \Omega_m^{0.6}$ (Peebles 1980). We use the Fourier transform (FT) convention defined as $\boldsymbol{v}(\boldsymbol{k}) = (1/V)\int_V d^3x \boldsymbol{v}(\boldsymbol{x}) e^{i\boldsymbol{k}\cdot\boldsymbol{x}}$ on a large volume V over which they are considered to be periodic. The inverse FT is thus defined as $\boldsymbol{v}(\boldsymbol{x}) = V/(2\pi)^3 \int d^3k \boldsymbol{v}(\boldsymbol{k}) e^{-i\boldsymbol{k}\cdot\boldsymbol{x}} = \sum_{\boldsymbol{k}} \boldsymbol{v}(\boldsymbol{k}) e^{-i\boldsymbol{k}\cdot\boldsymbol{x}}$.

From equation (4), the PS of velocity field (P_v) in the linear regime is related with the density PS (P_δ) as

$$P_v(k) = V\left\langle |\boldsymbol{v}(\boldsymbol{k})|^2\right\rangle = (DHf)^2 P_\delta(k)/k^2. \tag{5}$$

From the FT of equation (1), $\boldsymbol{p}(\boldsymbol{k}) = \boldsymbol{v}(\boldsymbol{k}) + \sum_{\boldsymbol{k}'} \delta(\boldsymbol{k}')\boldsymbol{v}(\boldsymbol{k}-\boldsymbol{k}')$, the approximate expression for the momentum PS is given by the sum of PS of $\boldsymbol{v}$ and $\delta\boldsymbol{v}$ fields (P00):

$$P_p(k) \approx P_v(k) + P_{\delta v}(k) = (DHf)^2 P_\delta(k)/k^2 + \frac{1}{2}(D^2Hf)^2 \int \frac{d^3k'}{(2\pi)^3}\frac{k^2}{k'^2|\boldsymbol{k}-\boldsymbol{k}'|^2} P_\delta(k') P_\delta(|\boldsymbol{k}-\boldsymbol{k}'|). \tag{6}$$

It should be noted that equation (6) is not a complete expression for the cosmic momentum PS because only the $\delta\boldsymbol{v}$ term is considered with the other non-linear terms excluded. Furthermore, equation (6) assumes that $\delta(\boldsymbol{x})$ and $\boldsymbol{v}(\boldsymbol{x})$ are Gaussian with a property that the ensemble of odd-product like $\langle\delta(\boldsymbol{x})\boldsymbol{v}(\boldsymbol{x})\cdot\boldsymbol{v}(\boldsymbol{x}+\boldsymbol{r})\rangle$ is zero. The correct expression for the momentum PS requires higher order perturbation theory (e.g., Bernardeau et al. 2002).

The accuracy of equation (6) can be tested using the N-body simulation data. Figure 1 shows the momentum and density PS directly measured from a N-body simulation of the ΛCDM cosmological model (open and filled circles). A particle-mesh code (Park 1990, 1997) is used to gravitationally evolve 256^3 CDM particles from $z = 23$ to 0 on a 512^3 mesh whose physical size is 614.4 h^{-1}Mpc. The cosmological parameters used in the simulation are $\Omega_m = 0.27$, $\Omega_b = 0.0463$, $\Omega_\Lambda = 0.73$, and $h = 0.72$,

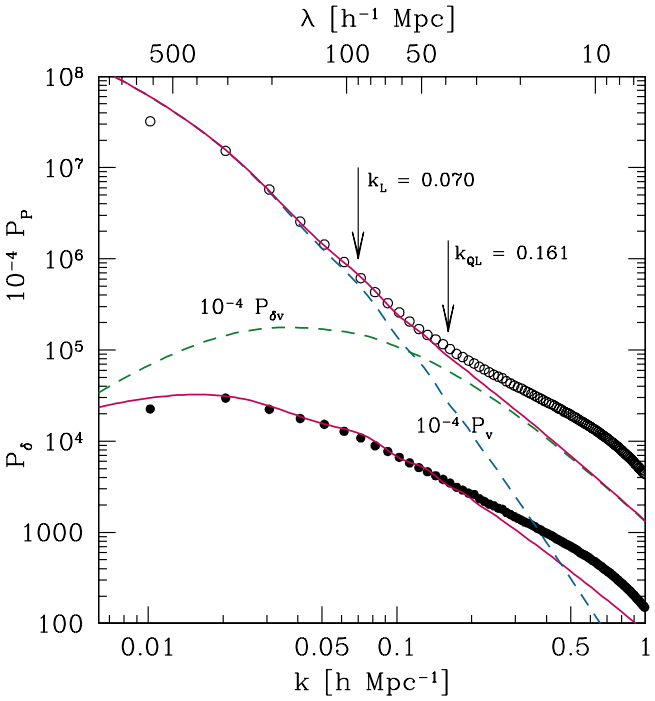

FIG. 1.— Momentum and density PS measured from the N-body simulation of the ΛCDM universe (open and filled circles), in units of km^{2}s^{-2}(h^{-1}Mpc)^3 and (h^{-1}Mpc)^3, respectively. The bottom solid curve is the linear matter density PS (P_δ) for ΛCDM cosmology as used in the N-body simulation. The upper solid curve denotes the momentum PS (P_p) that is the sum of PS of $\boldsymbol{v}$ and $\delta\boldsymbol{v}$ fields (P_v and $P_{\delta v}$; dashed curves). The P_v and $P_{\delta v}$ have been derived from the linear density PS (eq. [6]) The limits of the linear and the quasi-linear regimes, denoted as k_L and k_{QL}, respectively, are indicated as arrows (see §5).

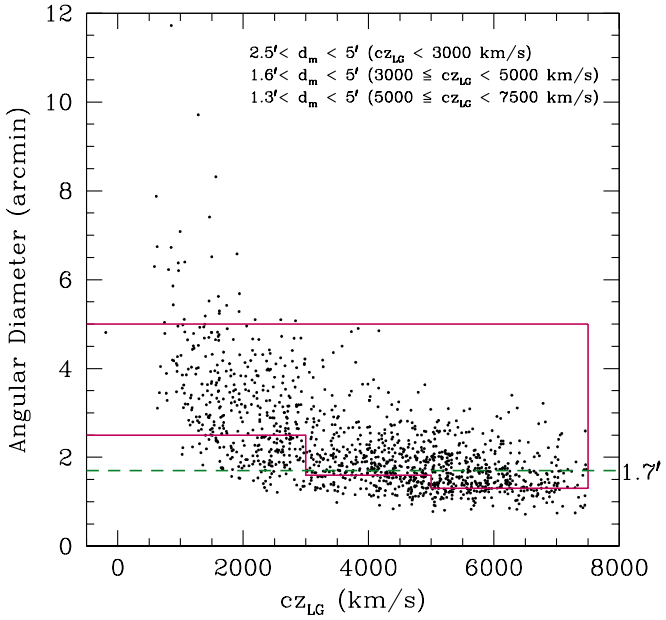

FIG. 2.— Redshift ($cz_{\rm LG}$) versus angular diameter (d_m) of 1289 galaxies in the SFI catalog. The d_m is obtained from a relation $d_m/a_{23.5} = 2.78 - 1.03\log(a/b)$, where $a_{23.5}$ is the isophotal angular radius measured at $\mu_I = 23.5$ mag/arcsec^2 level and a/b is the axial ratio. The region enclosed by solid lines represents the SFI main galaxy selection criteria, while the dashed line denotes our angular diameter limit applied to the second and the third redshift shells.

and the fitting formulae for PS given by Eisenstein & Hu (1999) are used. The simulation is normalized so that $\sigma_8 = 1/b = 0.9$ at $z = 0$, where σ_8 is the rms mass fluctuation within 8 h^{-1}Mpc sphere. We use the cloud-in-cell (CIC) scheme (e.g., Hockney & Eastwood 1981) in constructing density and momentum fields, and the fast Fourier transform (FFT) to estimate the PS. The upper solid curve which is the sum of PS of $\boldsymbol{v}$ and $\delta\boldsymbol{v}$ fields (two dashed curves) is the momentum PS calculated from equation (6) using the linear matter density PS (bottom solid curve). Comparison of the momentum PS measured from the N-body simulation (open circles) with the upper solid curve shows that the equation (6) is very accurate down to scales of about 50 h^{-1}Mpc (at the largest scale corresponding to the simulation box size, the agreement is not good because of the cosmic variance). This demonstrates that the momentum PS can be derived from the linear density PS even in the quasi-linear regime.

3. THE SFI GALAXY SAMPLE

3.1. *Description of the Sample*

The SFI galaxy catalog is an all-sky sample of peculiar velocity of galaxies. It contains 1289 Sbc–Sc galaxies with I-band TF distances (Giovanelli et al. 1994, 1997a,b; Haynes et al. 1999a,b). The galaxies in the catalog have inclination $i \gtrsim 45°$ and Galactic latitudes $|b| > 10°$. Its survey depth is $cz_{\rm LG} = 7500$ km/s, where $cz_{\rm LG}$ is the galaxy recession velocity with respect to the Local Group (LG). This sample is a combination of the SFI main galaxy sample ($\delta > -45°$) and Mathewson et al. (1992, hereafter MAT) sample of which the magnitudes and rotational velocities were converted to the SFI system.

The peculiar velocities of spiral galaxies in the SFI sample have been derived from the I-band TF relation. We consider the TF relation between the absolute magnitude M_I and the velocity width parameter η,

$$M_I = m_I - 5\log r = a_{\rm TF} + b_{\rm TF}\eta, \qquad (7)$$

where $\eta \equiv \log w - 2.5$ and w is the circular velocity line-width of a galaxy in unit of km/s. The absolute magnitude M_I is defined as the apparent magnitude when a galaxy is located at $r = 1$ km/s. For the slope and the zero-point of the TF relation, we adopt $a_{\rm TF} = -21.10$ and $b_{\rm TF} = -7.94$ of the inverse Tully-Fisher (ITF) relation that is determined by Giovanelli et al. (1997a) for 24 clusters in the SCI sample. The reason for using the ITF relation is worth mentioning. The forward TF relation is obtained by regressing the apparent magnitudes over the line-width. It can be biased due to the imposed selection limits on magnitude, angular diameter, and circular velocity line-width. On the other hand, the ITF relation is obtained by fitting the line-width as a function of the apparent magnitude. It avoids the selection bias if the sample selection is independent of the line-width (Strauss & Willick 1995; Freudling et al. 1995; Borgani et al. 2000a). We perform our analysis using the peculiar velocities inferred from the ITF relation. Borgani et al. (2000a) analyzes the SFI peculiar velocity data in redshift space to avoid the possible bias that can

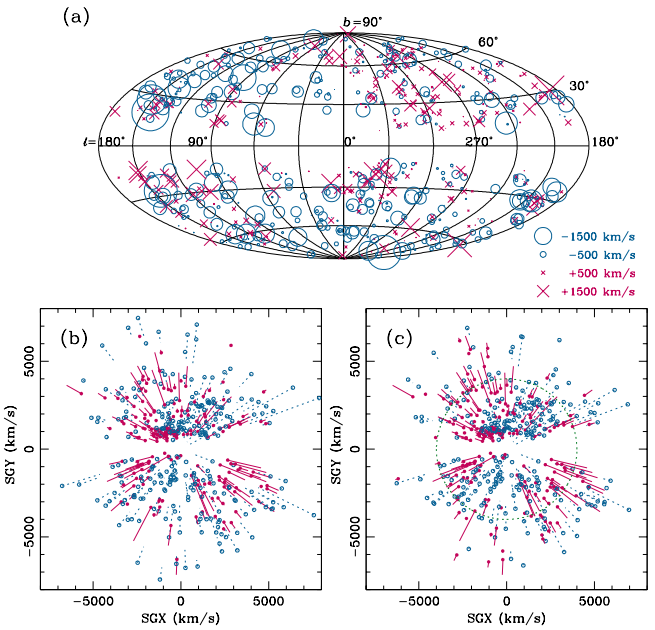

FIG. 3.— (*a*) Hammer-Aitoff sky projection in the Galactic coordinate as seen in the LG-frame, of the 661 SFI galaxies. Open circles indicate the infall while crosses outflow. The size of symbols scales with the velocity amplitude as shown in the bottom-right of the figure. (*b*) & (*c*) Distribution of the SFI galaxies in the supergalactic (SG) coordinates before and after MB correction, respectively. The positions and peculiar velocities are shown in the SGX–SGY plane with thickness of $\Delta Z < 2000$ km/s. Outflowing galaxies are denoted as dots with solid segments that scale with the velocity amplitude, while infalling galaxies as open circles with dotted segments. The large circle in panel (*c*) represents a region enclosed by a 40 h^{-1}Mpc sphere.

enter into the measurement of distances or peculiar velocities of galaxies. However, we make our analysis in *real* space to avoid the effects from the redshift space distortion.

The SFI galaxy sample, by desire, is angular-diameter limited. The sample was made to obtain roughly the same number of galaxies in three different redshift shells. Diameter limits imposed on the SFI main galaxy sample on each redshift shell are $2\farcm5 < d_m < 5'$ at $cz_{\rm LG} < 3000$ km/s, $1\farcm6 < d_m < 5'$ at $3000 \le cz_{\rm LG} < 5000$ km/s, and $1\farcm3 < d_m < 5'$ at $5000 \le cz_{\rm LG} < 7500$ km/s. Here d_m is the angular diameter defined as the UGC blue major axis or the analogous parameter in the ESO-Uppsala Survey (Giovanelli et al. 1994). The distribution of SFI galaxies on a $cz_{\rm LG}$–d_m plane is shown in Figure 2. The galaxies actually do not strictly follow the selection criteria. The angular diameter of each galaxy is estimated from a relation $d_m/a_{23.5} = 2.78 - 1.03\log(a/b)$, where $a_{23.5}$ is the I-band isophotal radius measured at $\mu_I = 23.5$ mag/arcsec^2 level and a/b is the axial ratio of a galaxy (Giovanelli et al. 1994). The angular diameter limit of the MAT galaxy sample is $1\farcm7$. For completeness of the SFI sample, we exclude galaxies with diameter smaller than $1\farcm7$ on the second and the third redshift shells. A small fraction of galaxies with small line-widths ($\log w < 2.25$) have also been discarded because of the large fractional errors in the measurement of their widths and thus the large uncertainties in the peculiar velocity measurement (da Costa et al. 1996). The total number of galaxies we use in our analysis is 661. Figure 3 shows the positions and peculiar velocities of the 661 SFI galaxies on the sky and the supergalactic plane. The supergalactic coordinate system is a Cartesian coordinate system with the SGZ-axis pointing to the Galactic coordinate $l = 47\fdg37$, $b = 6\fdg32$, and the SGX-axis pointing to $l = 137\fdg29$, $b = 0°$ (e.g., Peebles 1993).

3.2. *Bias Correction*

Real data are often selected by magnitude or diameter limits, and/or by redshift limit, which cause a bias in the calibration of the TF relation. This is particularly important for the SFI sample because the adopted redshift-dependent selection criteria imply that near each redshift limit outflowing galaxies are preferentially excluded from the sample. As shown in Figure 3*b* this effect becomes dominant at large distances, leading to a spurious systematic infall of galaxies at the outer edge of the survey volume (da Costa et al. 1996). In earlier studies with the SFI data, the biases were estimated using the numerical Monte-Carlo technique (Freudling et al. 1995; da Costa et al. 1996; Branchini et al. 2001) or using the semi-analytic approach (Freudling et al. 1999). In this paper, we incorporate all the selection effects into two selection functions: a radial function $\phi(r)$ for the redshift-dependent selection, and an angular function $\psi(b)$ for the Galactic extinction that may reduce the galaxy number density at the low Galactic latitude. For the radial selection function we use a method that is equivalent to the $V/V_{\rm max}$ method for computing the luminosity function (Schmidt 1968). The radial selection function $\phi(r)$ is given by (Park et al. 1994; Strauss & Willick 1995)

$$\phi(r) = \frac{3}{\Omega_s} \sum_{d_{{\rm max},i} > r} \frac{1}{d_{{\rm max},i}^3}, \qquad (8)$$

where Ω_s is the solid angle covered by the survey and $d_{{\rm max},i}$ is the maximum distance the i-th galaxy can have while satisfying the selection criteria.

Malmquist bias is caused by the random error in the galaxy distances estimated by the distance estimators like TF or D_n–σ relations (Lynden-Bell et al. 1988). At a given distance there are more galaxies that are perturbed from the far side than from the near side. The number of galaxies that are randomly moved to that distance also depends on the actual distribution of galaxies. Biases in the inferred distance or the peculiar velocity occur because of the volume effect and galaxy number density variation along the line of sight. We call the combination of the two effects the Malmquist bias (hereafter MB). To correct for MB, we have derived a density distribution of the local universe using the IRAS PSCz 0.6 Jy flux-limited catalog (Saunders et al. 2000). We assume the linear theory of gravitational instability to estimate the peculiar velocity of each PSCz galaxy, and obtain the real-space density field using the method described in Branchini et al. (1999). In deriving the density field we assume $\beta = 0.5$. Given a TF distance (d) of each galaxy, we obtain MB-corrected distance using a relation (Strauss & Willick 1995)

$$E(r|d) = \frac{\int_0^\infty r^3 n(r)\phi(r) \exp\left(-[\ln(r/d)]^2/2\Delta^2\right) dr}{\int_0^\infty r^2 n(r)\phi(r) \exp\left(-[\ln(r/d)]^2/2\Delta^2\right) dr}. \qquad (9)$$

Here $n(r)$ is the number density of galaxies along the line-of-sight, r denotes unbiased true distance, and $\Delta =$

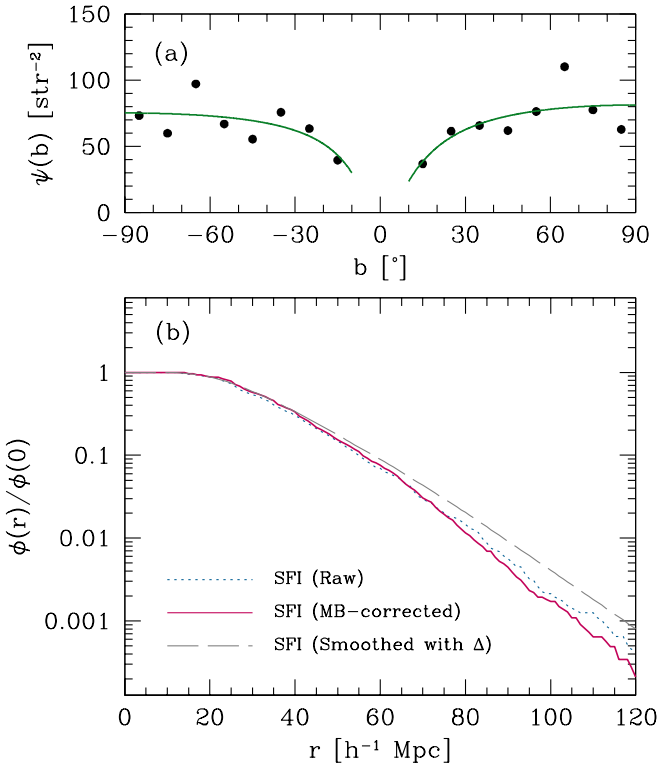

FIG. 4.— Angular (upper) and radial (bottom) selection functions of the 661 galaxies in the SFI sample. For the angular selection function we estimate the number density of galaxies at Galactic latitude bins with $\Delta b = 10°$. The estimated number densities have been fitted with a function $\psi(b) = \psi_0 10^{\alpha(1-\csc|b|)}$, where $\psi_0 = 81.3$ (75.2) and $\alpha = 0.113$ (0.084) for the northern (southern) hemisphere. Radial selection functions before and after MB correction, and that further smoothed with $\Delta = \sigma_{\rm TF} \ln 10/5$ are shown as dotted, solid, and dashed curves, respectively.

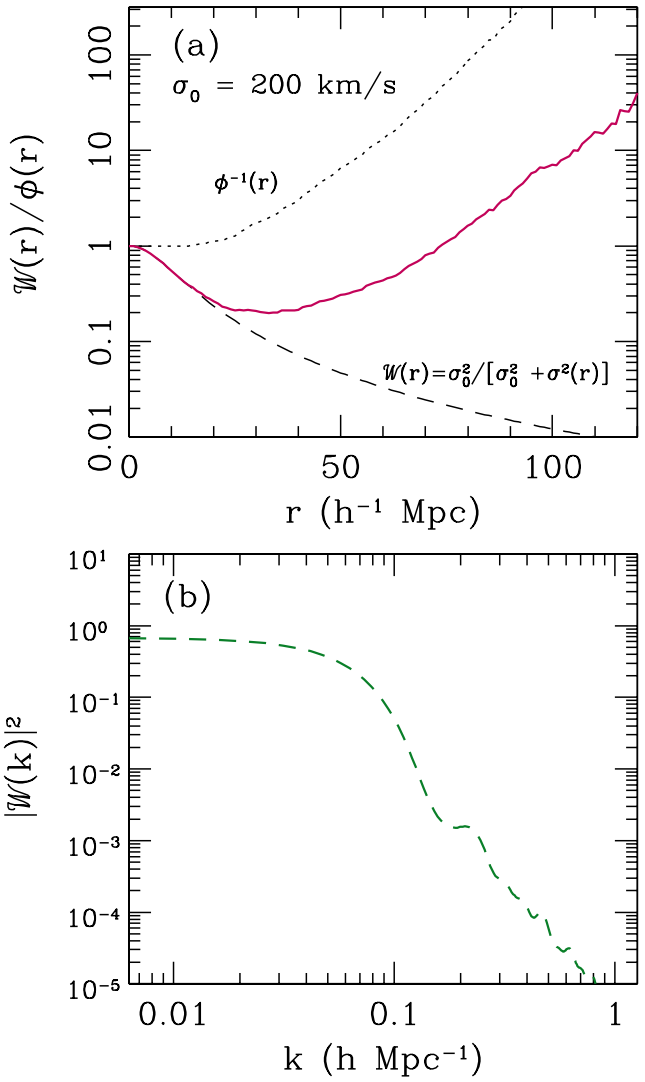

FIG. 5.— (Upper) Effective weight of a galaxy at distance r (solid curve), shown as the product of the inverse of the radial selection function ($\phi^{-1}(r)$; dotted) and the survey window function ($\mathcal{W}(r)$; dashed curve) for $\sigma_0 = 200$ km/s and $\sigma_{\rm TF} = 0.36$. Here $\phi(r)$ is normalized so that $\phi(0) = 1$. (Bottom) PS of the survey window function $|\mathcal{W}(\boldsymbol{k})|^2$. The survey region is limited to a volume within a sphere of $r_{\rm max} = 40\ h^{-1}$Mpc and $|b| > 10°$.

$\sigma_{\rm TF} \ln 10/5$ is a measure of the fractional distance uncertainty, where $\sigma_{\rm TF}$ is the error of the TF relation in unit of magnitude. In this paper, we assume $\sigma_{\rm TF} = 0.36$ (Giovanelli et al. 1997a). The $\phi(r)$ in equation (9) is the real-space radial selection function derived from the raw SFI sample (*not* corrected for MB; dotted curve in Fig. 4). Given the fully corrected distance estimate, $d_c = E(r|d)$, the radial component of the peculiar velocity is obtained as $u = cz_{\rm LG} - d_c$. The computed distances and peculiar velocities are used to measure the cosmic density and momentum PS (§4.3).

Figure 4 shows the angular and radial selection functions of the 661 galaxies in the SFI catalog. The angular selection function (ψ) is obtained by fitting the galaxy number density estimates at Galactic latitude bins to a function $\psi(b) = \psi_0 e^{\alpha(1-\csc|b|)}$. We calculate radial selection functions (ϕ) from the 661 galaxies before and after MB correction (dotted and solid curves, respectively), and MB-corrected selection function smoothed with a Gaussian filter of width Δ (dashed curve). The final selection function is given by $s(r, b) = \phi(r)\psi(b)$.

3.3. *Survey Window Function*

Although galaxy positions in redshift space are measured very accurately, the error in the absolute distances and the peculiar velocities of galaxies monotonically increases radially outward, and dominates the signal beyond a certain distance. The expected distance error of a galaxy at distance r (in h^{-1}Mpc) is approximately $\sigma(r) = 100r(e^{\Delta} - 1)$ km/s. To reduce the effects of the large distance error on the measured PS, we use a survey window function defined as

$$\mathcal{W}(r) = \frac{\sigma_0^2}{\sigma_0^2 + \sigma^2(r)}. \qquad (10)$$

With the smaller σ_0, the effective survey depth in our analysis becomes shallower. Figure 5 shows the inverse of radial selection function $\phi^{-1}(r)$ and the window function $\mathcal{W}(r)$ (dotted and dashed curves). The product $\phi^{-1}(r)\mathcal{W}(r)$, the solid curve in Figure 5*a*, is the effective weight of a galaxy at distance r (see eq. [12] in §4.1). We adopt $\sigma_0 = 200$ km/s and limit the sample depth to $r_{\rm max} = 40\ h^{-1}$Mpc to exclude distant galaxies with large

effective weights. The PS of the survey window function shown in Figure 5*b* is a monotonically and rapidly decreasing function, and is negligible at $k > 0.1\ h\mathrm{Mpc}^{-1}$. That is, the measured PS has correlations only within about $\Delta k = 0.1\ h\mathrm{Mpc}^{-1}$.

4. POWER SPECTRUM ESTIMATION

4.1. *Method*

In this section we describe the method of estimating the PS of the momentum field $P_p(k)$ from the observed radial peculiar velocity data. We use the PS estimation method developed by P00 (see also Park et al. 1994). The method uses a direct FT to calculate the Fourier modes of density and momentum fields. In this paper we slightly modify the direct FT method so that it can be applied to a case for an arbitrary window function.

Suppose we have N galaxies with positions $\boldsymbol{x}_j$ and radial peculiar velocities $u(\boldsymbol{x}_j)$, with $j = 1, \dots, N$. Owing to the variation of selection, each galaxy has a different statistical weight that is given by the inverse of the selection function, $w_j = s^{-1}(\boldsymbol{x}_j)$, where the sample selection function $s(\boldsymbol{x}_j)$ is defined to be the fraction of galaxies at position $\boldsymbol{x}_j$ expected to be observable by the survey. If the galaxies represent mass, the density contrast is related to the galaxy number density $n(\boldsymbol{x})$ as in

$$1 + \delta(\boldsymbol{x}) = \frac{n(\boldsymbol{x})}{\bar{n}} = \frac{1}{\sum_j w_j/V} \sum_j w_j \delta^{(3)}(\boldsymbol{x} - \boldsymbol{x}_j), \quad (11)$$

where $\delta^{(3)}(\boldsymbol{x} - \boldsymbol{x}_j)$ is the Dirac delta function, and V is the survey volume.

It is quite reasonable to assume that $\langle \boldsymbol{v} \rangle = 0$ for a sufficiently large volume. We estimate the mean peculiar velocity $\boldsymbol{v}_0$ using a bulk flow model for the radial peculiar velocities within $r_{\max}$. The mean velocity $\boldsymbol{v}_0$ is obtained by minimizing $\chi^2 = \sum_j \mathcal{W}_j^2 (u_j - \boldsymbol{v}_0 \cdot \hat{\boldsymbol{x}}_j)^2$, where $\mathcal{W}_j = \mathcal{W}(\boldsymbol{x}_j)$ and $u_j = u(\boldsymbol{x}_j)$, and $\hat{\boldsymbol{x}}_j$ is an unit vector pointing to the j-th galaxy (da Costa et al. 2000a). Then, we obtain a new radial peculiar velocity of each galaxy by subtracting a line-of-sight component of the mean peculiar velocity from the galaxy's observed radial peculiar velocity: $v_r(\boldsymbol{x}_j) = u(\boldsymbol{x}_j) - \boldsymbol{v}_0 \cdot \hat{\boldsymbol{x}}_j$.

The FT of the observed radial momentum field is

$$\begin{aligned} \hat{p}_r(\boldsymbol{k}) &= \frac{1}{V} \int d^3x \mathcal{W}(\boldsymbol{x}) \left[(1 + \delta(\boldsymbol{x})) \, \boldsymbol{v}(\boldsymbol{x}) \cdot \hat{\boldsymbol{x}} \right] e^{i\boldsymbol{k}\cdot\boldsymbol{x}} \\ &= \frac{1}{\sum_j w_j} \sum_{j=1}^{N} \mathcal{W}(\boldsymbol{x}_j) w_j v_r(\boldsymbol{x}_j) e^{i\boldsymbol{k}\cdot\boldsymbol{x}_j}. \end{aligned} \quad (12)$$

Likewise, the FT of $\delta(\boldsymbol{x})$ is given by $\hat{\delta}(\boldsymbol{k}) = \sum_j \mathcal{W}(\boldsymbol{x}_j) w_j e^{i\boldsymbol{k}\cdot\boldsymbol{x}_j} / \sum_j w_j - \mathcal{W}(\boldsymbol{k})$, where $\mathcal{W}(\boldsymbol{k})$ is the FT of the survey window function. The quantities with a caret, $\hat{p}_r(\boldsymbol{k})$ and $\hat{\delta}(\boldsymbol{k})$, are the momentum and density Fourier modes that are convolved with the survey window function. The ensemble average of $|\hat{p}_r(\boldsymbol{k})|^2$ is given by

$$\begin{aligned} &(\Sigma_j w_j)^2 \left\langle |\hat{p}_r(\boldsymbol{k})|^2 \right\rangle \\ &= \left\langle \sum_{j \in V} \mathcal{W}_j w_j v_{rj} e^{i\boldsymbol{k}\cdot\boldsymbol{x}_j} \sum_{m \in V} \mathcal{W}_m w_m v_{rm} e^{-i\boldsymbol{k}\cdot\boldsymbol{x}_m} \right\rangle \\ &= \sum_{j(\mathrm{cells})} \sum_{m(\mathrm{cells})} \mathcal{W}_j \mathcal{W}_m w_j w_m \left\langle n_j n_m v_{rj} v_{rm} \right\rangle e^{i\boldsymbol{k}\cdot(\boldsymbol{x}_j - \boldsymbol{x}_m)}, \end{aligned} \quad (13)$$

where $v_{rj} = v_r(\boldsymbol{x}_j)$. In the second equality, we divide the survey volume V into infinitesimal cells with occupation number $n_j = 0$ or 1. The ensemble averaged quantity $\langle n_j n_m v_{rj} v_{rm} \rangle$ is related with the radial momentum CF (ξ_{p_r}) as

$$\begin{aligned} &\langle n_j n_m v_{rj} v_{rm} \rangle \\ &= \begin{cases} \bar{n} s_j d^3 x_j \xi_{p_r}(0) & \text{if } j = m \\ \bar{n}^2 s_j s_m d^3 x_j d^3 x_m \xi_{p_r}(|\boldsymbol{x}_j - \boldsymbol{x}_m|) & \text{if } j \neq m \end{cases}, \end{aligned} \quad (14)$$

where $s_j = s(\boldsymbol{x}_j)$, and we use a property $\langle n_j \rangle = \bar{n} s_j d^3 x_j$. Similarly, for density PS we need to consider $\langle n_j n_m \rangle$. The right-hand side of equation (14) becomes $\sum_j w_j^2 \mathcal{W}_j^2 \xi_{p_r}(0)$ for $j = m$ case, and $(\sum_j w_j)^2 \sum_{\boldsymbol{k}'} |\mathcal{W}(\boldsymbol{k}')|^2 \left\langle |p_r(\boldsymbol{k} - \boldsymbol{k}')|^2 \right\rangle$ for $j \neq m$ case. The final formulae for the density and momentum field PS are

$$P_\delta(k) \approx V \left[\left\langle |\hat{\delta}(\boldsymbol{k})|^2 \right\rangle - \frac{\sum_j w_j^2 \mathcal{W}_j^2}{(\sum_j w_j)^2} \right] \Big/ \sum_{\boldsymbol{k}} |\mathcal{W}(\boldsymbol{k})|^2, \quad (15)$$

and

$$P_p(k) \approx 3V \left[\left\langle |\hat{p}_r(\boldsymbol{k})|^2 \right\rangle - \frac{\sum_j w_j^2 \mathcal{W}_j^2}{(\sum_j w_j)^2} \xi_{p_r}(0) \right] \Big/ \sum_{\boldsymbol{k}} |\mathcal{W}(\boldsymbol{k})|^2, \quad (16)$$

where the radial momentum CF at the zero lag can be estimated as

$$\xi_{p_r}(0) = \sum_j w_j^2 \mathcal{W}_j^2 v_{rj}^2 \Big/ \sum_j w_j^2 \mathcal{W}_j^2. \quad (17)$$

In equations (15) and (16), we assume that PS we are measuring are slowly varying functions, and approximate that the window-convolved PS ($\hat{P}$) can be separated into the true PS part (P) and the window-related part as $\hat{P}(k) \approx P(k) \sum_{\boldsymbol{k}} |\mathcal{W}(\boldsymbol{k})|^2$. The $\sum_{\boldsymbol{k}} |\mathcal{W}(\boldsymbol{k})|^2$ in the denominator is the overall power correction that compensates for power loss due to the finite window function that decreases radially outward.

4.2. *Momentum Power Spectrum from Mock Surveys*

We use the N-body simulation data in §2 to make mock SFI observations. To mimic the LG environment, we select an observer as a particle with total velocity 600–700 km/s on the over-dense region with $0 < \delta < 1$. From the chosen observer we randomly select the particles with probability given by $s(r, b)$. The radial selection is made at the true distance using the radial selection function derived from the MB-corrected SFI galaxy distribution (solid curve in Fig. 4). After the particle selection, we perturb the particle distances with Gaussian errors of Δ.

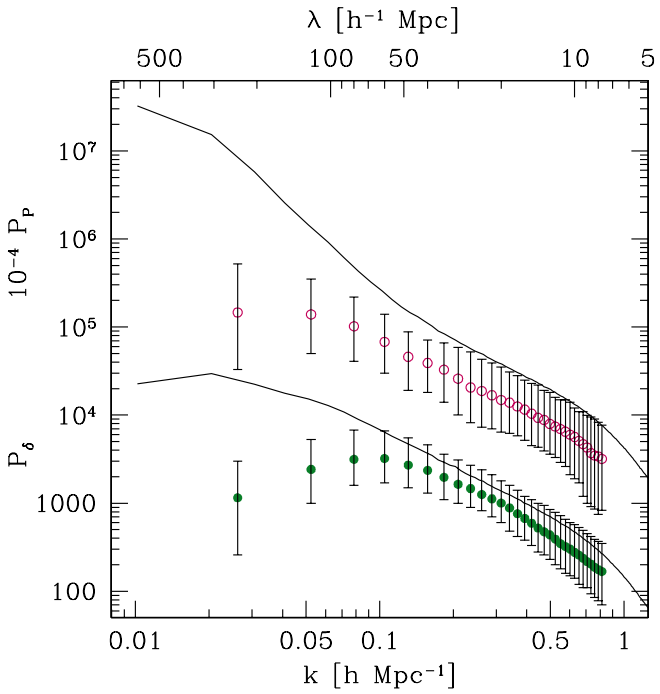

FIG. 6.— Momentum and density PS measured from 500 SFI mock observations. Shown are the median values (open and filled circles) and 68% confidence limits of the PS in the ΛCDM model. The solid curves are the true PS obtained from the N-body simulation data.

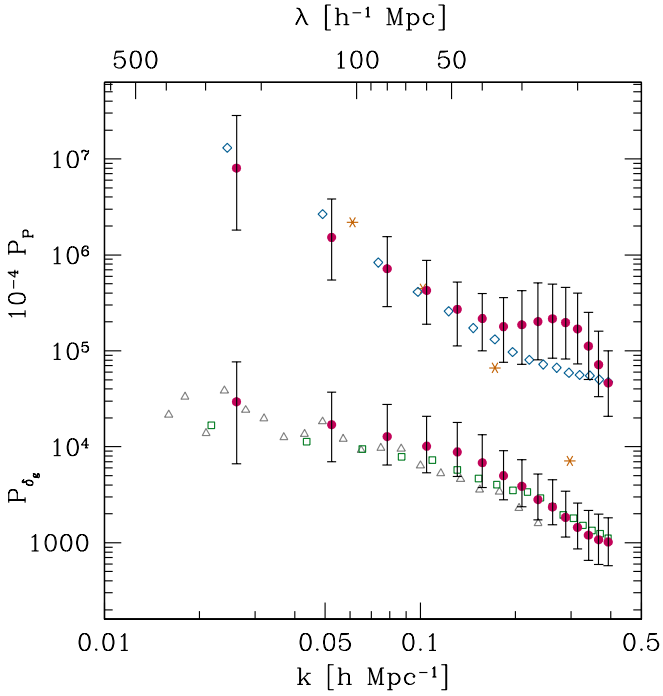

FIG. 7.— Momentum and density PS measured from the SFI galaxy sample (filled circles). The velocity PS measured from the Mark III catalog with POTENT method is shown as stars (Kolatt & Dekel 1997), and the momentum PS measured by P00 for the MAT data as diamonds. Open triangles denote the decorrelated real-space galaxy density PS measured from the SDSS galaxy redshift survey (Tegmark et al. 2004). Open squares represent the galaxy density PS in the real space calculated by Park et al. (1994) for the 101 h^{-1}Mpc deep subsample of the CfA survey.

By applying redshift cut at $cz_{\rm LG} = 7500$ km/s we finally obtain 661 angular positions and recession and peculiar velocities of 'galaxy' particles for each mock observation. For PS measurement, we use equation (9) to obtain the MB-corrected galaxy distances and peculiar velocities. Here we have smoothed the N-body simulation data to obtain $n(r)$ by applying a Gaussian filter with $\sigma = 5$ h^{-1}Mpc, and used the radial selection function smoothed with Δ (dashed curve in Fig. 4).

The PS of momentum and density fields measured from the five hundred SFI mock observations are shown in Figure 6. For each mock data the number of galaxies within $r_{\rm max} = 40$ h^{-1}Mpc varies from 300 to 400. Shown are the median values (open and filled circles) and 68% confidence limits of $P_p(k)$ (i.e., $3P_{p_r}(k)$) and $P_\delta(k)$ of the 500 SFI mock PS. Note that data points in the PS are correlated with each other over approximately four neighboring points ($\Delta k \simeq 0.1$ hMpc^{-1}). The solid curves are the true PS of momentum (upper) and density (bottom) fields of the ΛCDM universe measured from the N-body simulation (same as open and filled circles in Fig. 1). The damping of powers at large scales (or small k) occurs due to finiteness of the survey volume. Similar damping is also seen at high k, which is due to the smoothing effect of the peculiar velocity and distance errors. We use the ratio of the true PS to the PS of mock surveys as the correction factor when we measure the PS for the observed SFI sample. At each k, the raw power measured from the observed data is multiplied with the corresponding the correction factor. Then, the systematic effects in the raw powers are removed, and the PS with correct amplitudes can be restored. Those factors also reduce any residual biases. This method of correction for the systematic effects in the observed galaxy PS by using mock surveys has been developed by Park et al. (1992, 1994) and Vogeley et al. (1992).

4.3. *Application to the SFI Data*

We analyze the SFI catalog using the same method as applied to the mock SFI catalogs. The number of galaxies used in the analysis is 370 within $r_{\rm max} = 40$ h^{-1}Mpc. The final PS of the observed SFI galaxies obtained by multiplying the correction factor to the measured power spectrum at each k are shown in Figure 7 (filled circles). The PS are measured in the true distance space rather than in the redshift space. The 68% uncertainty limit at each wavenumber is estimated from the five hundred mock surveys in the ΛCDM model. The Poisson noise powers for the density and momentum PS are 523 $(h^{-1}{\rm Mpc})^3$ and 7.5×10^8 km^{2}s$^{-2}(h^{-1}{\rm Mpc})^3$, respectively. For comparisons, we plot the velocity PS measured by Kolatt & Dekel (1997) who applied the POTENT method to the Mark III catalog (stars), and the momentum PS measured by P00 for the MAT data (diamonds). The velocity field is close to linear at scales $k \lesssim 0.07$ hMpc^{-1}, where the momentum PS should be equal to the velocity PS (P00). We find that the velocity PS of Kolatt & Dekel is in good agreement with the SFI momentum PS only at the first two wavenumbers, while the MAT momentum PS is consistent with the SFI PS at all wavenumbers.

We also plot the real-space galaxy density PS for

the Sloan Digital Sky Survey (SDSS; open triangles; Tegmark et al. 2004) and the Center for Astrophysics (CfA; open squares; Park et al. 1994) galaxy samples. The measured SFI density PS is in good agreement with the SDSS and the CfA density PS even though the size of the SFI survey volume and the number of galaxies analyzed are much smaller. Compared to the SDSS and the CfA PS, the SFI density PS has relatively higher power at scales around 40 h^{-1}Mpc. The high power at those scales, considered to be a sampling effect due to the small survey volume, induces somewhat large value of $\sigma_{8,\rm S} = 1.14^{+0.33}_{-0.34}$, the rms mass fluctuation of the spiral galaxies within 8 h^{-1}Mpc sphere. The subscript S denotes the optical spiral galaxies. The 68% uncertainty limits are from the 500 mock surveys.

5. ESTIMATING THE β PARAMETERS

Until now, we have assumed that the galaxy distribution represents the mass field. If this is not true, the formulae containing the δ term should be modified because the observed momentum is now $(1+\delta_g)\boldsymbol{v}$. Suppose galaxies are linearly biased with respect to mass by a constant factor, i.e., $\delta_g = b\delta$, where b is the linear bias factor of galaxy distribution. In the linear regime the PS of velocity field in equation (5) becomes

$$P_v(k) = (H_0\beta)^2 P_{\delta_g}(k)/k^2, \qquad (18)$$

where $\beta = f(\Omega_m, \Omega_\Lambda)/b \simeq \Omega_m^{0.6}/b$ and P_{δ_g} is the galaxy density PS. P00 has proved that only the overall amplitude of the momentum PS given by equation (6) is scaled by a factor $\beta^2 = (f/b)^2$ due to biasing if β is independent of k.

Since we calculate both density and momentum PS from the same sample, it is possible to measure the β parameter more accurately. We estimate $\beta_{\rm S} = \Omega_m^{0.6}/b_{\rm S}$ parameter from the measured SFI PS. As observed by P00, there is a fair amount of correlation between the estimated P_δ and P_p. This is because density and momentum PS measured from the same sample tend to fluctuate statistically in a similar way. The correlation makes their ratios less uncertain, making the estimated β parameter more accurate. Furthermore, we note that the momentum PS can be derived from the observed density PS even in the quasi-linear regime (§1, Fig. 1). We estimate $\beta_{\rm S}$ from the following formula

$$\beta_{\rm S}(k) = \frac{P_p^{\rm obs}(k)}{P_p^{\rm der}(k)}. \qquad (19)$$

Here the derived momentum PS, $P_p^{\rm der}$, is calculated by equation (6) with the density PS replaced by $P_{\delta_g}^{\rm obs}$ and $D = f = 1$. During the numerical integration, we interpolate the density PS between the measured data points, and for small $k \lesssim 0.02$ hMpc^{-1} we extrapolate the PS using the ΛCDM linear density PS that has been scaled to match the observed PS. For large $k \gtrsim 1$ hMpc^{-1} we also extrapolate the PS by a power-law function that fits the observed PS at high k. Figure 8 shows the estimated $\beta_{\rm S}(k)$ at each wavenumber k with 68% limits including the cosmic variance (filled and open circles with error bars). The uncertainties have been determined from the distribution of $\beta_{\rm S}$ parameters of the 500 mock observations, where the PS of each mock observation are scaled to give the observed SFI PS on average.

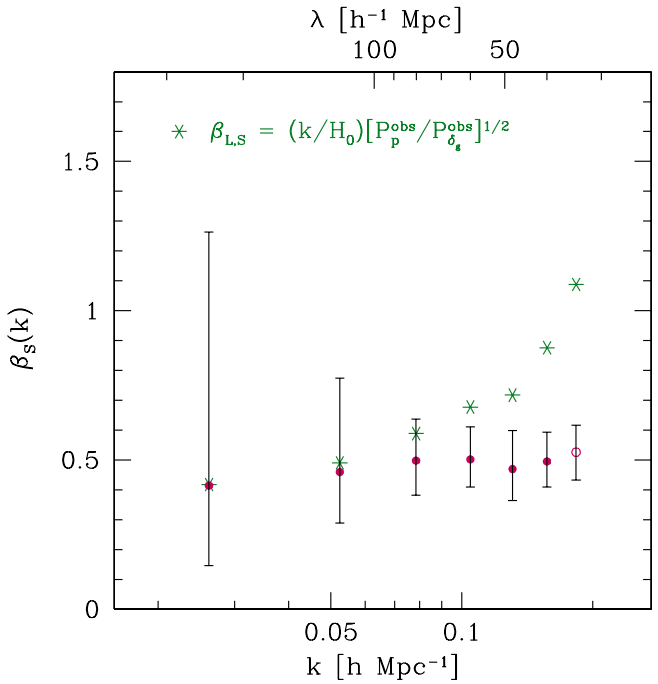

FIG. 8.— $\beta_{\rm S} = \Omega_m^{0.6}/b_{\rm S}$ parameters estimated from equation (19) (filled and open circles), together with $\beta_{L,\rm S}(k) = (k/H_0)[P_p^{\rm obs}(k)/P_{\delta_g}^{\rm obs}(k)]^{1/2}$ (stars). The uncertainties represents the 68% confidence limits which include the cosmic variance. The first six data points (filled circles) have been used to obtain the weighted average of $\beta_{\rm S}$ parameters (see Table 1).

We determine limits of the linear and quasi-linear regimes (k_L and k_{QL}) by comparing the true momentum PS with the velocity and momentum PS derived from the linear density PS (see Fig. 1). The k_L (k_{QL}) is defined as the scale at which the derived velocity (momentum) PS deviates from the true momentum PS (open circles in Fig. 1) by 20% in power. The two limits are $k_L = 0.070$ hMpc^{-1} and $k_{QL} = 0.161$ hMpc^{-1}, as denoted by arrows in Figure 1, and correspond to wavelengths of 90 and 39 h^{-1}Mpc, respectively. Table 1 lists the β parameters measured from the SFI galaxy sample in the range 0.0262 hMpc$^{-1} \le k \le 0.1571$ hMpc^{-1} (six filled circles in Fig. 8). The weighted average is $\beta_{\rm S} = 0.489^{+0.080}_{-0.050}$. We call $\beta_{L,\rm S}$ as β parameter calculated by using equation (18) in the linear scales $k \lesssim k_L$. They are also listed in Table 1, with a weighted average $\beta_{L,\rm S} = 0.55^{+0.29}_{-0.14}$. In estimating $\beta_{L,\rm S}$, we include β at 80 h^{-1}Mpc scale ($k = 0.0785$ hMpc^{-1}) where its uncertainty dominates over the 20% difference in power between the velocity and momentum PS. The $\beta_{L,\rm S}$ is very uncertain because the information contained in the survey volume is not enough to constrain the PS to an accurate value at large scales. It starts to deviate from $\beta_{\rm S}(k)$ significantly at $k > k_L$ where the linear gravitational instability theory no longer holds (see the stars in Fig. 8). In Figure 9 the observed SFI momentum PS (upper open circles) is compared with that derived from the observed density PS (diamonds) when $\beta = 0.489$. The momentum PS prediction is accurate on scales down to 40 h^{-1}Mpc.

Cosmological parameters derived from the momentum PS analysis are summarized in Table 2, where $\beta_{\rm S}$,

TABLE 1
$\beta_{\rm S} = \Omega_m^{0.6}/b_{\rm S}$ AND $\Omega_m^{1.2}P_\delta$ MEASURED FROM THE SFI PECULIAR VELOCITY SAMPLE

k (hMpc^{-1})	λ (h^{-1}Mpc)	$\beta_{L,{\rm S}}(k)^\dagger$	$\beta_{\rm S}(k)$	$\Omega_m^{1.2}P_\delta(k)$ $(h^{-1}{\rm Mpc})^3$
0.0262	240	$0.42^{+0.66}_{-0.20}$	$0.414^{+0.629}_{-0.198}$	$4.81^{+9.95}_{-4.00} \times 10^3$
0.0524	120	$0.49^{+0.30}_{-0.16}$	$0.459^{+0.272}_{-0.147}$	$3.50^{+3.68}_{-1.71} \times 10^3$
0.0785	80	$0.59^{+0.19}_{-0.13}$	$0.498^{+0.128}_{-0.106}$	$3.11^{+1.58}_{-1.06} \times 10^3$
0.1047	60	...	$0.502^{+0.103}_{-0.087}$	$2.51^{+0.91}_{-0.94} \times 10^3$
0.1309	48	...	$0.469^{+0.121}_{-0.099}$	$1.91^{+1.02}_{-0.78} \times 10^3$
0.1517	40	...	$0.495^{+0.096}_{-0.083}$	$1.65^{+0.75}_{-0.56} \times 10^3$
Average		$0.55^{+0.29}_{-0.14}$	$0.489^{+0.080}_{-0.050}$	...

NOTE. — $^\dagger\beta_{L,{\rm S}}(k) = (k/H_0)[P_p^{\rm obs}(k)/P_{\delta_g}^{\rm obs}(k)]^{1/2}$

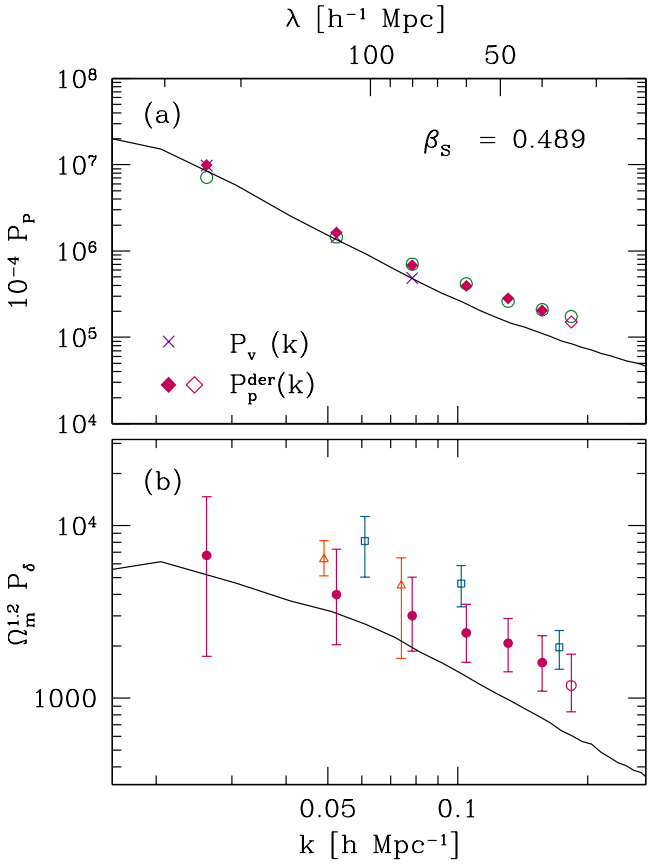

FIG. 9.— (Upper) Comparison of the observed momentum PS (open circles) for the SFI galaxy sample with the momentum PS ($P_p^{\rm der}$; diamonds) derived from the observed galaxy density PS ($P_{\delta_g}^{\rm obs}$) for $\beta_{\rm S} = 0.489$. The crosses are the velocity PS given by $P_v(k) = (H_0\beta_{\rm S})^2 P_{\delta_g}^{\rm obs}(k)/k^2$ for the SFI sample. (Bottom) Derived matter density PS given by $\Omega_m^{1.2}P_\delta(k) = \beta_{\rm S}^2 P_{\delta_g}^{\rm obs}(k)$ (circles). For comparisons, the matter density PS measured by Kolatt & Dekel (1997) for the Mark III sample (open squares) and by P00 for the MAT sample (open triangles) are plotted. The solid curves are the momentum and matter density PS calculated from the N-body simulation data of the ΛCDM universe.

TABLE 2
COSMOLOGICAL PARAMETERS DERIVED FROM THE MOMENTUM POWER SPECTRUM ANALYSIS

Parameters	Estimated Values
β measured from SFI sample	$\beta_{\rm S} = 0.49^{+0.08}_{-0.05}$
Matter density	$\Omega_m/b_{\rm S}^{5/3} = 0.30^{+0.09}_{-0.05}$
Rms mass fluctuation of spiral galaxies†	$\sigma_{8,{\rm S}} = 1.14^{+0.33}_{-0.34}$
Amplitude of mass fluctuation	$\sigma_8\Omega_m^{0.6} = 0.56^{+0.27}_{-0.21}$

NOTE. — †The rms mass fluctuation of the spiral galaxies within 8 h^{-1}Mpc sphere obtained by integrating the observed SFI density PS

$\Omega_m/b_{\rm S}^{5/3}$ $(= \beta_{\rm S}^{5/3})$, $\sigma_{8,{\rm S}}$, and $\sigma_8\Omega_m^{0.6}$ $(= \sigma_{8,{\rm S}}\beta_{\rm S})$ are listed with 68% confidence limits. Here the bias factor for optical spiral galaxies is defined to be $b_{\rm S} \equiv \sigma_{8,{\rm S}}/\sigma_8$. Table 3 compares our $\beta_{\rm S}$ and $\sigma_8\Omega_m^{0.6}$ measurements with the previous results obtained from spiral galaxy samples (SFI, MAT, and Mark III spirals). Compared with the previous studies with the SFI data, our $\beta_{\rm S}$ estimate is between those of Branchini et al. (2001) and da Costa et al. (1998), and our $\sigma_8\Omega_m^{0.6}$ between the large and the small values of Freudling et al. (1999) and Borgani et al. (2000a). By assuming that the bias factor is a function of k, given by $b_{\rm S}(k) = \left[P_{\delta_g}(k)/P_\delta(k)\right]^{1/2}$, we can infer the PS of mass fluctuation $\Omega_m^{1.2}P_\delta(k) = \beta_{\rm S}^2(k)P_{\delta_g}(k)$, by multiplying the observed density PS by $\beta_{\rm S}^2(k)$ at each k (Table 1). In Figure 9 we plot the PS of mass fluctuation given by $\Omega_m^{1.2}P_\delta(k) = \beta_{\rm S}^2 P_{\delta_g}^{\rm obs}(k)$ with $\beta_{\rm S} = 0.489$ (filled and open circles in the bottom panel). For comparisons, the matter density powers measured from the Mark III (Kolatt & Dekel 1997; open squares) and the MAT (P00; open triangles) samples are also shown. The MAT mass fluctuation powers are in good agreement with our estimates while those of Mark III sample are higher than ours on 60–100 h^{-1}Mpc scales.

To assess the effects of MB correction on the β estimation, we have measured the momentum and density PS using the SFI data that are *not* corrected for MB. The measured density PS has amplitudes very similar to that

TABLE 3
COMPARISON OF $\beta_{\rm S}$ AND $\sigma_8\Omega_m^{0.6}$ DERIVED FROM THE SPIRAL GALAXY SAMPLES

$\beta_{\rm S}$	$\sigma_8\Omega_m^{0.6}$	Data	Method	Ref.
$0.49^{+0.08}_{-0.05}$	$0.56^{+0.27}_{-0.21}$	SFI	Mom. PS	This Study
0.6 ± 0.1	···	SFI, IRAS 1.2 Jy	OME	1
0.42 ± 0.04	···	SFI, IRAS PSCz	VELMOD	2
···	0.82 ± 0.12	SFI	ML	3
···	$(0.3 \pm 0.1)[\Gamma/0.2]^{1/2}$	SFI	CF	4
···	0.63 ± 0.08	SFI	ML	5
$0.51^{+0.13}_{-0.08}$	0.56 ± 0.21	MAT	Mom. PS	6
0.6 ± 0.125	···	MAT	ROBUST	7
0.50 ± 0.10	···	Mark III (S), IRAS 1.2 Jy	OME	8
0.49 ± 0.07	···	Mark III (S), IRAS 1.2 Jy	VELMOD	9
$0.60^{+0.13}_{-0.11}$	···	Mark III (S)	$V_{\rm rms}$	10

REFERENCES. — (1) da Costa et al. (1998); (2) Branchini et al. (2001); (3) Freudling et al. (1999); (4) Borgani et al. (2000a); (5) Silberman et al. (2001); (6) Park (2000); (7) Rauzy & Hendry (2000); (8) Davis et al. (1996); (9) Willick et al. (1997b); (10) Padilla & Lambas (1999)

NOTE. — Γ is the shape parameter of the CDM models.

from the SFI data with MB correction, but the measured momentum PS has lower amplitudes at all scales. The β parameter, estimated in the same way as described above, decreases to 0.393, which is about 2σ below our estimation $\beta_{\rm S} = 0.489$. There are systematic effects on β estimation from errors in peculiar velocities and distances of galaxies. To measure the size of systematic effects, we have calculated β parameters using the mock catalogs with *true* distances and peculiar velocities. The estimated 68% uncertainty limits are $(-0.13, +0.24)$ and $(-0.048, +0.053)$ for $\beta_{L,{\rm S}}$ and $\beta_{\rm S}$, respectively. They are very similar to but slightly smaller than those for the realistic SFI mock catalogs. This indicates that the uncertainty of β for the SFI sample is still dominated by the statistical effect rather than systematic effects.

6. DISCUSSION

We have measured the momentum and density PS from the SFI peculiar velocity data, and estimated $\beta_{\rm S} = \Omega_m^{0.6}/b_{\rm S}$ parameter and the amplitude of mass fluctuation $\sigma_8\Omega_m^{0.6}$. Our method is self-consistent because only the SFI peculiar velocity sample is used without relying on other external velocity or density fields. By noting that the momentum PS is accurately related to the galaxy density PS up to the quasi-linear regime (§2, Fig. 1) and that the density and momentum PS measured from the same sample fluctuate in a similar way, we have estimated β parameter over a wide range of wavenumber space. We have determined limits of the linear and the quasi-linear regimes as $k_L = 0.070\ h{\rm Mpc}^{-1}$ and $k_{QL} = 0.161\ h{\rm Mpc}^{-1}$, and over the ranges $k \lesssim k_L$ and $k \lesssim k_{QL}$ we have estimated $\beta_{L,{\rm S}}$ and $\beta_{\rm S}(k)$, respectively. Our $\beta_{\rm S}$ estimation gives stable and consistent values around 0.5 at scales from 240 h^{-1}Mpc to 40 h^{-1}Mpc (Fig. 8 and Table 1), with an average $\beta_{\rm S} = 0.49^{+0.08}_{-0.05}$, which translates into the matter density parameter $\Omega_m = 0.30^{+0.09}_{-0.05} b_{\rm S}^{5/3}$. Our measurement is consistent with β parameter estimates from other studies with spiral galaxy samples, and is more accurate. Especially, the derived parameters are very similar to those from P00 who has applied the momentum PS analysis method to the MAT sample.

Table 4 summarizes β or mass fluctuation measurements of other studies that use different peculiar velocity samples (ellipticals, spirals plus ellipticals, and Type Ia supernovae). In β estimation, most of studies depend on the external galaxy distribution information such as IRAS 1.2 Jy and PSCz catalogs for comparing the observed peculiar velocities with that derived from the galaxy redshift survey data (v-v comparison), and give β parameters around 0.5. However, the POTENT method, one of the δ-δ comparison methods, usually gives much higher value of β parameter (Kolatt & Dekel 1997; Sigad et al. 1998). Compared with Kolatt & Dekel (1997), our momentum PS is consistent with their velocity PS in the linear regime (Fig. 7). Despite this fact, their estimate of the β parameter is much higher than ours. This is because Kolatt & Dekel (1997) have used the density PS from other redshift surveys in estimating β. Recently, Zaroubi et al. (2002) have applied UMV estimator to SEcat, a combination of the SFI and the ENEAR catalogs, and found consistent β estimates from both δ-δ and v-v comparison methods. Interestingly, low β estimation ($\beta = 0.2$–0.4) has been reported by Riess et al. (1997) and Blakeslee et al. (1999) who have compared the Optical Redshift Survey (ORS; Santiago et al. 1995) with peculiar velocities from Type Ia supernovae and a surface brightness fluctuation (SBF) survey of galaxy distances, respectively.

Our measurement of the mass fluctuation level $\sigma_8\Omega_m^{0.6} = 0.56^{+0.27}_{-0.21}$ is larger than that derived from the Wilkinson Microwave Anisotropy Probe (WMAP; Bennett et al. 2003) data analysis. Spergel et al. (2003) have used WMAP data to derive a value of $\sigma_8\Omega_m^{0.6} = 0.44 \pm 0.10$. The reason for the large $\sigma_8\Omega_m^{0.6}$ is that our measurement of the rms fluctuation of galaxy distribution gives somewhat large and uncertain value $\sigma_{8,{\rm S}} =$

TABLE 4
COMPARISON OF β AND $\sigma_8\Omega_m^{0.6}$ DERIVED FROM THE OTHER PECULIAR VELOCITY SAMPLES

Parameter	Data	Method	Ref.
	β		
0.50 ± 0.10	ENEAR, IRAS PSCz	OME (v-v)	1
$0.51^{+0.06}_{-0.06}$	SEcat, IRAS PSCz	UMV (v-v)	2
$0.57^{+0.11}_{-0.13}$	SEcat, IRAS PSCz	UMV (δ-δ)	2
0.50 ± 0.04	Mark III, IRAS 1.2 Jy	VELMOD (v-v)	3
1.20 ± 0.10	Mark III, IRAS 1.2 Jy	POTENT (δ-δ)	4
0.89 ± 0.12	Mark III, IRAS 1.2 Jy	POTENT (δ-δ)	5
0.50 ± 0.06	D_n–σ, IRTF, ESO, UGC	χ^2 fit. (v-v)	6
0.39 ± 0.17	SMAC, IRAS PSCz	χ^2 fit. (v-v)	7
0.40 ± 0.15	SNIa, IRAS 1.2Jy	χ^2 fit. (v-v)	8
0.30 ± 0.10	SNIa, ORS	χ^2 fit. (v-v)	8
0.55 ± 0.06	SNIa, IRAS PSCz	χ^2 fit. (v-v)	9
$0.42^{+0.10}_{-0.06}$	SBF, IRAS 1.2 Jy	χ^2 fit. (v-v)	10
0.26 ± 0.08	SBF, ORS	χ^2 fit. (v-v)	10
	$\sigma_8\Omega_m^{0.6}$		
$0.50^{+0.25}_{-0.14}$	SCI	$V_{\rm rms}$	11
$0.51^{+0.24}_{-0.09}$ for $\Gamma = 0.25$	ENEAR	CF	12
$1.1^{+0.2}_{-0.35}$	ENEAR	ML	13
0.88 ± 0.15	Mark III	ML	14
0.49 ± 0.06	Mark III	ML	15
(0.71–0.77)$\pm$0.12	Mark III	POTENT	4

REFERENCES. — (1) Nusser et al. (2001); (2) Zaroubi et al. (2002); (3) Willick & Strauss (1998); (4) Kolatt & Dekel (1997); (5) Sigad et al. (1998); (6) Hudson (1994); (7) Hudson et al. (2004); (8) Riess et al. (1997); (9) Radburn-Smith et al. (2004); (10) Blakeslee et al. (1999); (11) Borgani et al. (1997) (12) Borgani et al. (2000b); (13) Zaroubi et al. (2001); (14) Zaroubi et al. (1997); (15) Silberman et al. (2001)

$1.14^{+0.33}_{-0.34}$. By assuming that WMAP cosmological parameters $\sigma_8 = 0.9$ and $\Omega_m = 0.29$, we obtain $\sigma_{8,\rm S} = \sigma_8\Omega_m^{0.6}/\beta_{\rm S} = 0.87^{+0.10}_{-0.13}$ for $\beta_{\rm S} = 0.489$. Despite the higher amplitude of mass fluctuation than the WMAP value, our estimation of the matter density PS $\Omega_m^{1.2}P_\delta(k)$ is lower than those of other studies (Table 1 and Fig. 9). For example, at $k = 0.1047\ h{\rm Mpc}^{-1}$ ($\lambda = 60\ h^{-1}$Mpc), our PS value is $\Omega_m^{1.2}P_\delta(k) = 2.51^{+0.91}_{-0.94} \times 10^3\ (h^{-1}{\rm Mpc})^3$, which is lower compared with the high-amplitude power spectra found from the ML analyses of all-sky peculiar velocity samples such as Mark III, SFI, and ENEAR. At $k = 0.1\ h{\rm Mpc}^{-1}$ scale, the matter density powers ($\Omega_m^{1.2}P_\delta$) from the ML analyses are $(4.8 \pm 1.5) \times 10^3$ (Mark III; Zaroubi et al. 1997), $(4.4 \pm 1.7) \times 10^3$ (SFI; Freudling et al. 1999), and $(6.5 \pm 3) \times 10^3\ (h^{-1}{\rm Mpc})^3$ (ENEAR; Zaroubi et al. 2001). Those analyses also give the high mass fluctuation levels ($\sigma_8\Omega_m^{0.6}$) around 0.8–1.1 (Table 3 and 4). On the contrary, Silberman et al. (2001) found a power deficiency at $k = 0.1\ h{\rm Mpc}^{-1}$ from the ML analysis of the SFI sample, and their density PS and $\sigma_8\Omega_m^{0.6}$ are consistent with our results.

As shown in Figure 8, the β in the quasi-linear regime is more accurate than that in the linear-regime. This implies that if we rely on the linear regime where the density and velocity PS are simply related by the linear gravitational instability theory as in equation (5), we need peculiar velocity data with large survey volume for accurate determination of the β parameter. On the other hand, if we use the full information of the momentum field from linear to quasi-linear regimes where the relation between the density and momentum PS are accurately known, a peculiar velocity sample gives more accurate β compared with that estimated only in the linear regime. For the best β determination, it is essential to derive a more accurate relation that connects the density PS with the momentum PS beyond the limit of the quasi-linear regime by applying the higher order perturbation theory.

We gratefully acknowledge to Dr. Riccardo Giovanelli and Dr. Martha Haynes for providing the SFI galaxy sample. CGP acknowledges valuable comments from Kin-Wang Ng and Juhan Kim. This work was supported by the Astrophysical Research Center for the Structure and Evolution of the Cosmos (ARCSEC) of the Korea Science and Engineering Foundation (KOSEF) through Science Research Center (SRC) program.

REFERENCES

Bennett, C.L., et al. 2003, ApJS, 148, 1

Bernardeau, F., Colombi, S., Gaztañaga, E., & Scoccimarro, R. 2002, Phys. Rep. 367, 1

Bertschinger, E., Dekel, A., Faber, S.M., Dressler, A., & Burstein, D. 1990, ApJ, 364, 370
Blakeslee, J.P., Davis, M., Tonry, J.L., Dressler, A., & Ajhar, E.A. 1999, ApJ, 527, L73
Borgani, S., da Costa, L.N., Freudling, W., Giovanelli, R., Haynes, M.P., Salzer, J., & Wegner, G. 1997, ApJ, 482, L121
Borgani, S., da Costa, L.N., Zehavi, I., Giovanelli, R., Haynes, M.P., Freudling, W., Wegner, G., & Salzer, J.J. 2000a, ApJ, 119, 102
Borgani, S., Bernardi, M., da Costa, L.N., Wegner, G., Alonso, M.V., Willmer, C.N.A., Pellegrini, P.S., & Maia, M.A.G. 2000b, ApJ, 537, L1
Branchini, E., et al. 2001, MNRAS, 326, 1191
Branchini, E., et al. 1999, MNRAS, 308, 1
da Costa, L.N., Bernardi, M., Alonso, M.V., Wegner, G., Willmer, C.N.A., Pellegrini, P.S., Maia, M.A.G., & Zaroubi, S. 2000a, ApJ, 537, L81
da Costa, L.N., Bernardi, M., Alonso, M.V., Wegner, G., Willmer, C.N.A., Pellegrini, P.S., Rité, C., & Maia, M.A.G. 2000b, AJ, 120, 95
da Costa, L.N., Freudling, W., Wegner, G., Giovanelli, R., Haynes, M.P., & Salzer, J.J. 1996, ApJ, 468, L5
da Costa, L.N., Nusser, A., Freudling, W., Giovanelli, R., Haynes, M.P., Salzer, J.J., & Wegner, G. 1998, MNRAS, 299, 425
Davis, M., Nusser A., & Willick, J.A. 1996, ApJ, 473, 22
Dekel, A., Eldar, A., Kolatt, T., Yahil, A., Willick, J.A., Faber, S.M., Courteau, S., & Burstein, D. 1999, ApJ, 522, 1
Eisenstein, D.J., & Hu, W. 1999, ApJ, 511, 5
Feldman, H., et al. 2003, ApJ, 596, L131
Freudling, W., da Costa, L.N., Wegner, G., Giovanelli, R., Haynes, M.P., & Salzer, J.J. 1995, AJ, 110, 920
Freudling, W., et al. 1999, ApJ, 523, 1
Giovanelli, R., Haynes, M.P., Salzer, J.J., Wegner, G., da Costa, L.N., & Freudling, W. 1994, AJ, 107, 2036
Giovanelli, R., Haynes, M.P., Herter, T., Vogt, N.P., da Costa, L.N., Freudling, W., Salzer, J.J., & Wegner, G. 1997a, AJ, 113, 53
Giovanelli, R., Haynes, M.P., Herter, T., Vogt, N.P., Wegner, G., Salzer, J.J., da Costa, L.N., & Freudling W. 1997b, AJ, 113, 22
Górski, K., Davis, M., Strauss, M.A., White, S.D.M., & Yahil, A. 1989, ApJ, 344, 1
Haynes, M.P., Giovanelli, R., Chamaraux, P., da Costa, L.N., Freudling, W., Salzer, J.J., & Wegner, G. 1999a, AJ, 117, 2039
Haynes, M.P., Giovanelli, R., Salzer, J.J., Wegner, G., Freudling, W., da Costa, L.N., Herter, T., & Vogt, N.P. 1999b, AJ, 117, 1668
Hockney, R.W., & Eastwood, J.W. 1981, Computer Simulation Using Particles (New York: McGraw-Hill, 1981)
Hudson, M.J. 1994, MNRAS, 266, 475
Hudson, M.J., Smith, R.J., Lucey, J.R., & Branchini, E. 2004, MNRAS, 352, 61
Kolatt, T., & Dekel, A. 1997, ApJ, 479, 592
Lynden-Bell, D., Faber, S.M., Burstein, D., Davies, R.L., Dressler, A., Terlevich, R.J., & Wegner, G. 1988, ApJ, 326, 19
Mathewson, D.S., Ford, V.L., & Buchhorn, M. 1992, ApJS, 81, 413 (MAT)
Nusser, A., da Costa, L.N., Branchini, E., Bernardi, M., Alonso, M.V., Wegner, G., Willmer, C.N.A., & Pellegrini, P.S. 2001, MNRAS, 320, L21
Nusser, A., & Davis, M., 1995, MNRAS, 276, 1391
Padilla, N., & Lambas, D.G. 1999, MNRAS, 310, 21
Park, C. 1990, MNRAS, 242, 59p
Park, C. 1997, J. Korean Astron. Soc., 30, 191
Park, C. 2000, MNRAS, 319, 573 (P00)
Park, C., Gott, J.R., & da Costa, L.N. 1992, ApJ, 392, L51
Park, C., Vogeley, M.S., Geller, M.J., & Huchra, J.P. 1994, ApJ, 431, 569
Peebles, P.J.E. 1980, The Large-Scale Structure of the Universe (Princeton University Press)
Peebles, P.J.E. 1993, Principles of Physical Cosmology (Princeton University Press)
Radburn-Smith, D.J., Lucey, J.R., & Hudson, M.J. 2004, MNRAS, 355, 1378
Rauzy, S., & Hendry, M.A. 2000, MNRAS, 316, 621
Riess, A.G., Davis, M., Baker, J., & Kirshner, R.P. 1997, ApJ, 488, L1
Santiago, B.X., Strauss, M.A., Lahav, O., Davis, M., Dressler, A., & Huchra, J.P. 1995, ApJ, 446, 457
Saunders, W., et al. 2000, MNRAS, 317, 55
Schmidt, M. 1968, ApJ, 151, 393
Sigad, Y., Eldar, A., Dekel, A., Strauss, M.A., & Yahil, A. 1998, ApJ, 495, 516
Silberman, L., Dekel, A., Eldar, A., & Zehavi, I. 2001, ApJ, 557, 102
Spergel, D.N., et al. 2003, ApJS, 148, 175
Strauss, M.A., & Willick, J.A. 1995, Phys. Rep., 261, 271
Tegmark, M., et al. 2004, ApJ, 660, 702
Vogeley, M.S., Park, C., Geller, M.J., & Huchra, J.P. 1992, ApJ, 391, L5
Watkins, R., Feldman, H.A., Chambers, S.W., Gorman, P., & Melott, A.L. 2002, ApJ, 564, 534
Willick, J.A., Courteau, S., Faber, S.M., Burstein, D., Dekel, A., & Strauss, M.A. 1997, ApJS, 109, 333
Willick, J.A., & Strauss, M.A. 1998, ApJ, 507, 64
Willick, J.A., Strauss, M.A., Dekel, A., & Kolatt, T. 1997, ApJ, 486, 629
Zaroubi, S. 2002, in Proceedings of XIII Rencontres de Blois, Frontiers of the Universe, ed. L.M. Celnikier et al. p.65 (astro-ph/0206052)
Zaroubi, S., Bernardi, M., da Costa, L.N., Hoffman, Y., Alonso, M.V., Wegner, G., Willmer, C.N.A., & Pellegrini, P.S. 2001, MNRAS, 326, 375
Zaroubi, S., Branchini, E., Hoffman, Y., & da Costa, L.N. 2002, MNRAS, 336, 1234
Zaroubi, S., Hoffman, Y., & Dekel, A. 1999, ApJ, 520, 413
Zaroubi, S., Zehavi, I., Dekel, A., Hoffman, Y., & Kolatt, T. 1997, ApJ, 486, 21